Optical Materials 104 (2020) 109843

Contents lists available at ScienceDirect

Optical Materials

journal homepage: http://www.elsevier.com/locate/optmat

Luminescence of monoclinic Y_2O_3:Eu nanophosphor produced via laser vaporization

A.I. Kostyukov [a], V.N. Snytnikov [a,b], Vl.N. Snytnikov [b], A.V. Ishchenko [a,b], M.I. Rakhmanova [a,c], M.S. Molokeev [d,e,f], A.S. Krylov [d], A.S. Aleksandrovsky [d,g,*]

[a] Novosibirsk State University, Pirogova Str. 2, 630090, Novosibirsk, Russia
[b] Boreskov Institute of CatalysisSB RAS, Lavrentieva Ave. 5, 630090, Novosibirsk, Russia
[c] Nikolaev Institute of Inorganic Chemistry SB RAS, Akad. Lavrentiev Ave. 3, 630090, Novosibirsk, Russia
[d] Kirensky Institute of Physics Federal Research Center KSC SB RAS, Krasnoyarsk, 660036, Russia
[e] Siberian Federal University, Krasnoyarsk, 660041, Russia
[f] Department of Physics, Far Eastern State Transport University, Khabarovsk, 680021, Russia
[g] Department of Photonics and Laser Technology, Siberian Federal University, Krasnoyarsk, 660041, Russia

ARTICLE INFO

Keywords:
Photoluminescence of Eu^{3+}
Monoclinic Y_2O_3:Eu nanophosphor
Laser vaporization

ABSTRACT

Europium doped Y_2O_3spherical nanoparticles with the diameter ~10 nmobtained via cw laser vaporization are shown to crystallize in monoclinic symmetry class (*C2/m* space group). The size of nanoparticles established via HRTEM coincides with coherent scattering region established by XRD. Luminescence spectrum in the vicinity of ultranarrow transition demonstrates three peaks consistent with three inequivalent positions of Eu^{3+} ion in monoclinic Y_2O_3 lattice. Hypersensitive transition dominates in the spectrum, admitting the lack of inversion symmetry at C_s sites occupied by Eu^{3+}. The spectrum of hypersensitive transition is expanded to the red part of spectrum due intense transitions terminating at higher-lying components of crystal-field-split $^7F_2$ energy level. Obtaining chromaticity coordinates (0.669, 0.331)and absolute quantum yield (~21%) is possible using red phosphor based on monoclinic Y_2O_3:Eu^{3+}.

1. Introduction

Investigations of new red phosphors are presently extremely abundant area of materials research. Prominent progress is achieved with Eu^{2+} ion in different hosts including nitrides (see e.g. Ref. [1,2] and references therein) and oxides [3–5] via crystal field engineering of the spectral shift of f-d emission of this ion. The choice of the host crystal structure and variation of chemical content of some already investigated hosts for Eu^{2+} ions allows wide tuning of color properties of divalent europium phosphors as well as resulting solid state lighting sources based on them. Red phosphors based on trivalent europium were extensively investigated in the past, and commercial phosphors were created, one of them being Y_2O_3:Eu^{3+} with cubic crystal structure. Spectral properties of trivalent europium luminescence are controllable by the choice of host, too, but to the much smaller extent than those of divalent europium. In the particular, chromaticity coordinates of commercial cubic Y_2O_3: Eu^{3+} (position of maximum $\lambda = 612$ nm)are (0.645, 0.352) that is not well suitable for some applications.

Chromaticity of phosphors based on trivalent europium is determined by the distribution of intensities between luminescent bands originating from higher-lying $^5D_0$ energy level and terminating at low-lying ^7F_J ($J = 0 \ldots 6$) states. Hypersensitive transition to $^7F_2$ state typically is dominating in efficient phosphors since its maximum oscillator strength induced by crystal field is favorable to combat radiationless losses. Distribution of intensities of transitions between individual crystal-field-split subcomponents within this band varies from the host to host, and typically the maximum of emission lies between 610 and 620 nm. (For several recent examples of shaping the spectra of trivalent europium see e.g. Ref. [6] (612 and 616 nm) [7], (611 nm) [8], (613.9 nm)). Very peculiar shaping of spectra was obtained in Ref. [7,8] where solitary line is completely dominating over the rest of $^5D_0$ - $^7F_2$ band that may be useful for obtaining laser generation in materials with similar crystalline structure. However, chromaticity in new hosts investigated in Ref. [6–8]is not suitable for illumination purposes. Attractive results in tailoring the luminescence spectrum of trivalent europium were obtained in $Ba_2Gd_2Si_4O_{13}$ [9]

* Corresponding author. Kirensky Institute of Physics Federal Research Center KSC SB RAS, Krasnoyarsk, 660036, Russia.
E-mail address: aleksandrovsky@kirensky.ru (A.S. Aleksandrovsky).

https://doi.org/10.1016/j.optmat.2020.109843
Received 6 February 2020; Received in revised form 5 March 2020; Accepted 19 March 2020
Available online 28 March 2020

where chromaticity coordinates (0.66, 0.34) were reported.

Oxides of rare earth elements, including yttrium, can crystallize in several crystalline structures, including cubic (*Ia*3), hexagonal ($P\bar{3}m1$) and monoclinic (*C*2/*m*) [10]. Monoclinic polymorphs can be obtained under the high pressure but the transition is irreversible. Properties of europium in these crystalline structures are not studied in detail up to date. Recently monoclinic nanocystalline Y_2O_3 is investigated in Ref. [11], however, luminescence of Eu^{3+} impurity was not analyzedin detail. Luminescence of monoclinic Y_2O_3:Eu^{3+} nanoparticles obtained by one step flame pyrolysis was investigated in Ref. [12], and the modification of Eu^{3+} luminescence spectra in the monoclinic polymorph with respect to the cubic one was demonstrated. Laser vaporization approach is often used for obtaining the nanoparticles, too, and it is featured by some peculiarities i.e., possibility to control the properties of nanoparticles by laser intensity on the target and by the variation of particle condensation conditions (gas composition, pressure, gas flow rate). Monoclinic Y_2O_3:Eu^{3+} nanoparticles were recently obtained via pulsed1 micron Yb fiber laser evaporation [13]. Quite different regime of vaporization takes place when the laser wavelength falls into the spectral region of lattice vibrations of the target. The aim of the present study is to obtainnanoparticles of europium doped monoclinic polymorph of Y_2O_3 (m-Y_2O_3:Eu^{3+}) via cw CO_2laser vaporizationin argon flow, and to investigate the spectral properties of obtained nanophosphor with the help of high-resolution spectroscopy.

2. Experimental techniques

2.1. Synthesis of europium doped m-Y_2O_3 nanoparticles

Y_2O_3:Eu nanoparticles were obtained by laser vaporization of $Y_{1.9}Eu_{0.1}O_3$ ($T_{cal.}$ = 850 °C/4h) ceramic targets irradiated by a cw CO_2 laser (radiation wavelength 10.6 μm, generation power up to 110 W on one TEM_{00} transverse mode, output beam diameter 8 mm, divergence in the far-field region 3×10^{-3} rad) with subsequent condensation of vapor in an Ar (99.99%) buffer gas flow in a vaporization chamber. Laser power on the target surface was 103 W (the power density 5.5×10^4 W/cm^2). A detailed description of a setup used for the synthesis of nanomaterials can be found in the Supporting Information and in Ref. [14, 15].

2.2. Characterization

Elemental analysis of the samples was made using X-ray fluorescence spectroscopy (XRF) on an ARL – Advant'x analyzer with the Rh anode of the X-ray tube. The morphology of the synthesized samples was characterized by high-resolution transmission electron microscopy (HRTEM) on a JEM-2010 electron microscope at accelerating voltage 200 kV and resolution 1.4 Å. Samples were deposited on a copper grid by dispersing a solid phase suspension in alcohol using an ultrasonic disperser.

The powder diffraction data of Y_2O_3:Eu and of pure Y_2O_3 initial cubic compound for Rietveld analysis were collected at room temperature with a Bruker D8 ADVANCE powder diffractometer (Cu-Kα radiation) and linear VANTEC detector. The step size of 2θ was 0.016°, and the counting time was 2 s per step.

High-resolution luminescence spectra were obtained using Horiba Jobin Yvon T64000 spectrometer and GaN laser excitation source at the central wavelength 408 nm. Absolute quantum yield of solid sample (PLQYs) measurements were performed using a Fluorolog 3 (Horiba Jobin Yvon) spectrofluorometer equipped with a 450 W ozone-free Xe lamp, a R-928 photomultiplier and a spectralone covered G8 integration sphere (GMP SA, Switzerland).

3. Results and discussion

3.1. HRTEMand XRD results

As shown by the elemental analysis performed by XRF, after vaporization of the $Y_{1.9}Eu_{0.1}O_3$ ceramic target and subsequent condensation of vapor, europium enters the composition of the produced Y_2O_3 nanoparticles with the close concentration.

Fig. 1 displays HRTEM images of the nanosized Y_2O_3:Eu sample. TEM images of Y_2O_3:Eu sample demonstrate that particles have a spherically symmetric shape and are represented by nanocrystallites with the mean size $d_m = 11.7 \pm 6.3$ nm. HRTEM images of the sample show interplanar distances that can be attributed mainly to monoclinic Y_2O_3:Eu (PDF# 87-2361).

All peaks of powder pattern were indexed by monoclinic cell (*C*2/*m*) with parameters close to Sm_2O_3 [16]. Therefore this structure was taken as starting model for Rietveld refinement which was performed using TOPAS 4.2 [17]. Sm ions at all three inequivalent sites were changed to Y ions in thestarting model before refinement. In order to reduce number of refined parameters, only one thermal parameter was refined for all O atoms. Refinement was stable and gave low *R*-factors (Table 1, Fig. 2a). Coordinates of atoms and main bond lengths are in Table 2 and Table 3 respectively. Estimated nanocrystal size from refinement was equal to 9.3(3) nm, in good agreement with HRTEM results. Initial compound was fitted by well-known cubic *Ia*-3 phase (Table 1, Fig. 2b). Possible content of cubic polymorph in the nanocrystalline sample can be estimated to be below 5%. Crystal structure of monoclinic polymorph is presented in Fig. 3.

3.2. Luminescence

Fig. 4 presents overall high-resolution luminescence spectrum of m-Y_2O_3:Eu^{3+}(red line) in comparison with that of reference crystal α-$Eu_2(MoO_4)_3$ [18] (blue line). The characteristic bands of Eu^{3+}luminescence in of obtained nanophosphor are in general the same as in Ref. [13] except for certain minor differences specified below.

Crystal-field-induced electric dipole band $^5D_0$ - $^7F_2$ dominates over magnetic dipole band $^5D_0$ - $^7F_1$ in this spectrum, indicating sufficient degree of inversion symmetry violation in the local environment of trivalent europium ion. The ratio of intensities of crystal-field-induced $^5D_0$ - $^7F_2$and magnetic dipole $^5D_0$ - $^7F_1$bands is not so large as in the case of reference crystal, however, estimates show that obtaining high quantum efficiency with m-Y_2O_3:Eu^{3+} is quite feasible in case of sufficiently small non-radiative losses. The spectral region of ultranarrow transition of trivalent europium ion is presented in Fig. 5 in more detail.

In contrast to the spectrum of reference crystal with its single inequivalent position of europium ion, local symmetry of which being C_1, the spectrum of m-Y_2O_3:Eu^{3+} exhibits three peaks in the region of $^5D_0$ - $^7F_0$ transition that is consistent with three inequivalent positions for Y in crystal structure of monoclinic Y_2O_3 polymorph, the local symmetry of all three being C_s. Note that only two peaks in the area of ultranarrow transition were observed in Ref. [13] and the authors of the latter study deduced that two of three peaks coincide in ther nanoparticles. The maxima of these $^5D_0$ - $^7F_0$ transitions are positioned at 579.9, 580.1 and 581.9 nm; therefore, energies of $^5D_0$ states are 17,272, 17238.3 and 17184.8 cm^{-1}. The narrowest of $^5D_0$ - $^7F_0$ lines must be associated with octahedral site of Y within m-Y_2O_3 structure while two others must be ascribed to sites with monocapped trigonal prism local environment. The width of peak at 581.9 nm equals to 11.2 cm^{-1}, being 3.5 times wider than ultranarrow peak in α-$Eu_2(MoO_4)_3$ (3.1 cm^{-1}). This broadening must be ascribed to size broadening of luminescence lines observed in nanoparticles. The peak at 581.9 nm exceeds the peaks of neighboring $^5D_0$ - $^7F_1$ transition that means rather high degree of violation of mirror symmetry at its site. The spectral structure of $^5D_0$ - $^7F_2$ band is shown in Fig. 6 in more detail.

The maxima of this band are positioned at 615 and 623 nm, the latter

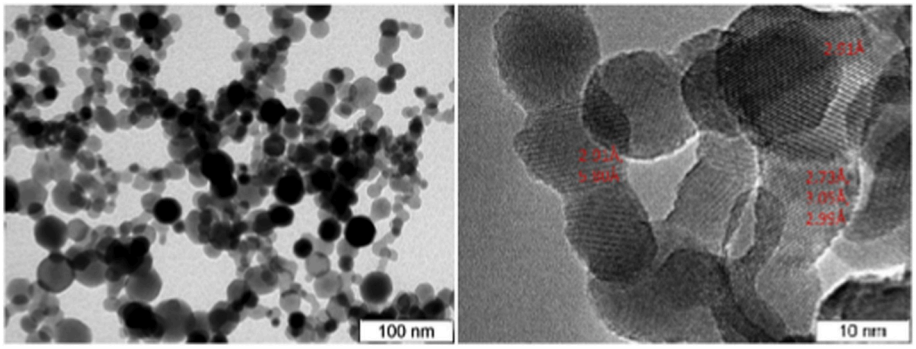

Fig. 1. HRTEM images of Y_2O_3:Eu sample with interplanar spacing.

Table 1
Main parameters of processing and refinement of the m-Y_2O_3:Eu and c-Y_2O_3samples.

Compound	Y_2O_3:Eu	Y_2O_3 initial
Sp.Gr.	*C2/c*	*Ia-3*
a, Å	13.964 (2)	10.823 (2)
b, Å	3.5009 (6)	–
c, Å	8.6308 (17)	–
β, °	100.185 (9)	–
V, Å^3	415.30 (13)	1267.8 (7)
Z	6	16
2*θ*-interval, °	5–140	5–100
R_{wp}, %	3.71	3.01
R_p, %	2.88	2.18
R_{exp}, %	2.53	2.03
χ^2	1.46	1.48
R_B, %	0.74	0.84

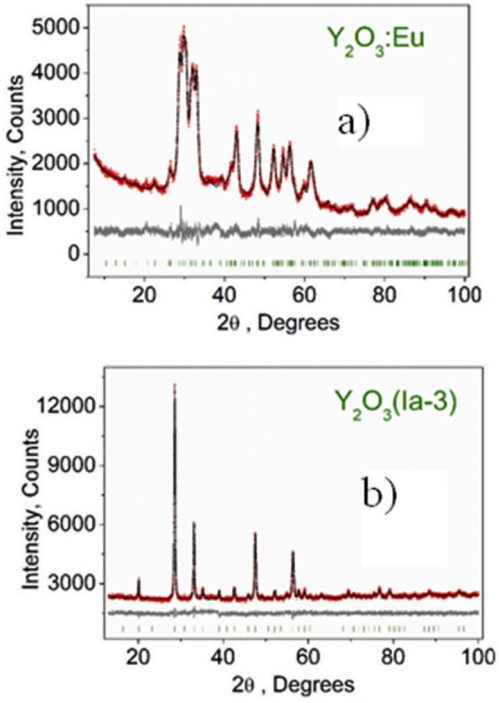

Fig. 2. Difference Rietveld plot of: a) nanoparticles of m-Y_2O_3:Eu; b) cubic Y_2O_3. Grey line is the difference between experimental and simulated patterns.

being of even higher height, and additional longer-wavelength peaks exist with wings protruding up to 635 nm. This part of spectrum is present in cubic Y_2O_3:Eu^{3+} but its amplitude in c-Y_2O_3:Eu^{3+} is less than

Table 2
Fractional atomic coordinates and isotropic displacement parameters (Å^2) of Y_2O_3:Eu.

Atom	Wyckoff site	Local symmetry	*x*	*y*	*z*	B_{iso}
Y1	4*i*	*m*	0.1337 (4)	0.5	0.4876 (5)	0.5 (7)
Y2	4*i*	*m*	0.1887 (4)	0.5	0.1427 (6)	0.7 (7)
Y3	4*i*	*m*	0.4642 (5)	0.5	0.1864 (7)	0.3 (7)
O1	4*i*	*m*	0.115 (2)	0	0.333 (2)	1.2 (8)
O3	4*i*	*m*	0.2740 (19)	0.5	0.365 (4)	1.2 (8)
O4	4*i*	*m*	0.465 (2)	0	0.333 (3)	1.2 (8)
O5	2*b*	2/*m*	0	0.5	0	1.2 (8)
O2	4*i*	*m*	0.327 (2)	0.5	0.029 (3)	1.2 (8)

Table 3
Main bond lengths (Å) of Y_2O_3:Eu.

Y1—O1	2.188 (11)	Y2—O5	2.704 (5)
Y1—O3	2.39 (2)	Y2—O2	2.32 (2)
Y1—O3^{i}	2.40 (2)	Y2—O2^{iii}	2.279 (17)
Y1—O4^{ii}	2.49 (2)	Y3—O1^{iv}	2.26 (2)
Y1—O4^{i}	2.25 (3)	Y3—O4	2.159 (15)
Y2—O1	2.724 (16)	Y3—O5^{iv}	2.487 (4)
Y2—O3	2.07 (3)	Y3—O2	2.14 (3)

Symmetry codes: (i) -*x*+1/2, *y*+1/2, -*z*+1; (ii) *x*-1/2, *y*+1/2, *z*; (iii) -*x*+1/2, *y*+1/2, -*z*; (iv) *x*+1/2, *y*+1/2, *z*.

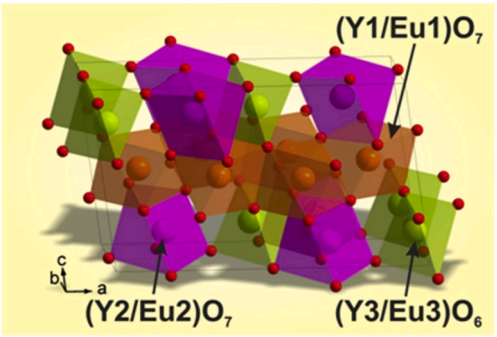

Fig. 3. Crystal structure of monoclinic Y_2O_3:Eu with three inequivalent positions for Y/Eu.

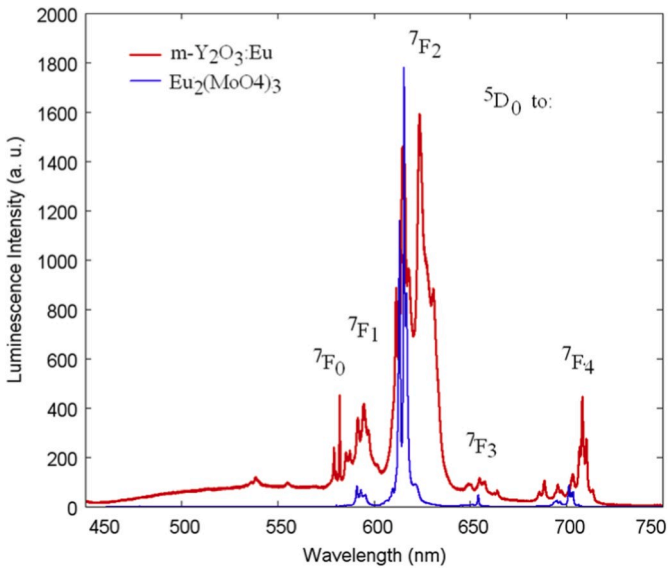

Fig. 4. Overall luminescence spectrum of m-Y_2O_3:Eu excited at 408 nm (red) in comparison with the luminescence of α-$Eu_2(MoO_4)_3$ (blue). Luminescence bands originate from $^5D_0$ starting level and terminate at ^7F_J levels as indicated. (For interpretation of the references to color in this figure legend, the reader is referred to the Web version of this article).

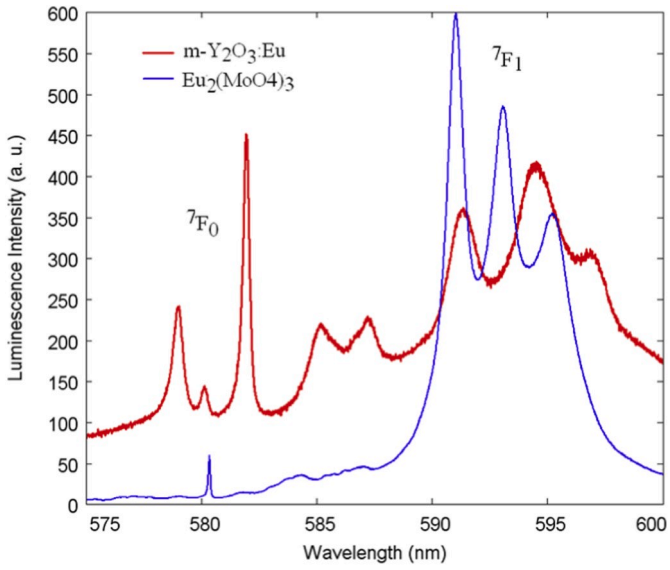

Fig. 5. Luminescence spectrum in the vicinity of ultranarrow transition for m-Y_2O_3:Eu excited at 408 nm (red) in comparison with the luminescence of α-$Eu_2(MoO_4)_3$ (blue). (For interpretation of the references to color in this figure legend, the reader is referred to the Web version of this article).

in m-Y_2O_3:Eu^{3+}. Additional subbands in the spectral range from 620 to 635 nm within $^5D_0$ - $^7F_2$ luminescent band of m-Y_2O_3:Eu^{3+}must be ascribed to the transitions from $^5D_0$ in three inequivalent sites to highest components of crystal-field-split $^7F_2$ manifold.

In addition to emission originating from $^5D_0$ state, weak emission from $^5D_1$ to $^7F_{0,1,2}$ is detectable in the spectrum of m-Y_2O_3:Eu^{3+}presented in Fig. 4. One may notice that narrow Eu^{3+} emission bands are observed above the background that is represented by broad band from 460 to 720 nm with the maximum approximately at 600 nm. This band must be assigned to the presence of divalent europium in m-Y_2O_3 nanoparticles. Note that divalent europium was detected, e.g., in nanoparticles of cubicY_2O_3obtained via coprecipitation [19]. The

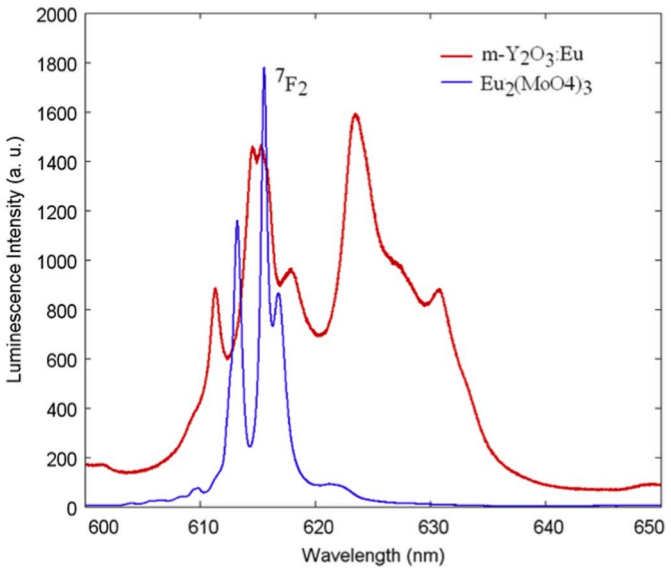

Fig. 6. Luminescence band terminating at $^7F_2$ energy level for m-Y_2O_3:Eu excited at 408 nm (red) in comparison with that of α-$Eu_2(MoO_4)_3$ (blue). (For interpretation of the references to color in this figure legend, the reader is referred to the Web version of this article).

excitation maximum is expected to lie in the UV, and observed emission is the long-wavelength wing of the whole possible emission band of divalent europium. Nevertheless, this contribution strongly affects the chromaticity coordinates of m-Y_2O_3:Eu nanophosphor. Calculation over the whole emission range of m-Y_2O_3: Eu results in (0.582 0.381) chromaticity coordinates, while calculation over emission range of Eu^{3+} ion results in (0.669, 0.331) ones. The latter values are desired for some applications, for instance they are very close to the standard recommended by NTSC. Therefore, complete stabilization of Eu^{3+} valence state in m-Y_2O_3 is promising for creation of new standard source of red color, while optimization of Eu^{3+}/Eu^{2+} content and of the excitation wavelength is the potential way for creation of white phosphor.

The QY measured using integrating sphere for the monoclinic Y_2O_3:Eu^{3+} pumped at 395 nm was 21%, while for our home-made cubic Y_2O_3:Eu^{3+} ceramics this value was 30%. Before measuring the QY of m-Y_2O_3:Eu nanoparticles it were annealed at 600 °C for 4 h in air to remove water and organic molecules and also to reduce the concentration of anion vacancies. According to the XRD data, the nanoparticles at this annealing temperature kept their monoclinic structure and nanoparticles size. The QY of the m-Y_2O_3:Eu^{3+} nanophosphor is strongly dependent on the Eu^{3+} concentration, particle size, PL quenching and crystallinity of the nanophosphor. Therefore, there is reason to believe that in the future, the optimization of these parameters will allow obtaining a higher QY.

4. Conclusion

Europium doped Y_2O_3 nanoparticles were obtained via cw CO_2-laser evaporation. XRD analysis shows that laser evaporation enables crystallization of Y_2O_3 in the crystal structure belonging to monoclinic symmetry class (*C2/m* space group). HRTEM evidences formation of spherical nanoparticles with the diameter of order of 10 nm and with good crystallinity. Luminescence spectrum in the vicinity of ultranarrow transition demonstrates three peaks consistent with three inequivalent positions of Eu^{3+} ion in monoclinic Y_2O_3 lattice. Hypersensitive transition dominates in the spectrum admitting the lack of inversion symmetry at C_s sites occupied by Eu^{3+}. The spectrum of hypersensitive transition is broadened to the red part of spectrum due intense transitions terminating at higher-lying components of crystal-field-split $^7F_2$ energy level. Obtaining chromaticity coordinates (0.669, 0.331) and

absolute quantum yield (~21%) is possible using red phosphor based on monoclinic Y_2O_3:Eu^{3+}.

Declaration of competing interest

The authors declare that they have no known competing financial interests or personal relationships that could have appeared to influence the work reported in this paper.

CRediT authorship contribution statement

A.I. Kostyukov: Conceptualization, Investigation, Writing - original draft. **V.N. Snytnikov:** Investigation. **Vl.N. Snytnikov:** Investigation. **A.V. Ishchenko:** Investigation. **M.I. Rakhmanova:** Investigation. **M.S. Molokeev:** Formal analysis. **A.S. Krylov:** Investigation. **A.S. Aleksandrovsky:** Conceptualization, Formal analysis, Writing - original draft.

Acknowledgment

This work is financially supported by the Russian Foundation for Basic Research № 19-32-60027. Use of equipment of Krasnoyarsk Regional Center of Research Equipment of Federal Research Center«-Krasnoyarsk Science Center SB RAS»is acknowledged.

Appendix A. Supplementary data

Supplementary data to this article can be found online at https://doi.org/10.1016/j.optmat.2020.109843.

References

[1] M.-H. Fang, S. Mahlik, A. Lazarowska, M. Grinberg, M.S. Molokeev, H.-S. Sheu, J.-F. Lee, R.-S. Liu, Angew. Chem. Int. Ed. 58 (23) (2019) 7767.
[2] C.C. Lin, Y.-T. Tsai, H.E. Johnston, M.-H. Fang, F. Yu, W. Zhou, P. Whitfield, Y. Li, J. Wang, R.-S. Liu, J.P. Attfield, J. Am. Chem. Soc. 139 (2017), 11766.
[3] M. Zhao, Y. Zhou, M.S. Molokeev, Q. Zhang, Q. Liu, Z. Xia, Adv. Opt. Mater. 7 (2019), 180163, 1.
[4] M. Zhao, H. Liao, M.S. Molokeev, Y. Zhou, Q. Zhang, Q. Liu, Z. Xia, Light Sci. Appl. 8 (38) (2019) 1.
[5] H. Liao, M. Zhao, M.S. Molokeev, Q. Liu, Z. Xia, Angew. Chem. 57 (36) (2018), 11728.
[6] Y.G. Denisenko, V.V. Atuchin, M.S. Molokeev, A.S. Aleksandrovsky, A.S. Krylov, A. S. Oreshonkov, S.S. Volkova, O.V. Andreev, Inorg. Chem. 57 (21) (2018), 13279.
[7] V.V. Atuchin, A.K. Subanakov, A.S. Aleksandrovsky, B.G. Bazarov, J.G. Bazarova, T.A. Gavrilova, A.S. Krylov, M.S. Molokeev, A.S. Oreshonkov, S. Yu Stefanovich, Mater. Des. 140 (2018) 488.
[8] V.V. Atuchin, A.S. Aleksandrovsky, B.G. Bazarov, J.G. Bazarova, O.D. Chimitova, Y.G. Denisenko, T.A. Gavrilova, A.S. Krylov, E.A. Maximovskiy, M.S. Molokeev, A. S. Oreshonkov, A.M. Pugachev, N.V. Surovtsev, J. Alloys Compd. 785 (2019) 692.
[9] H. Guo, H. Zhang, R.F. Wei, M.D. Zheng, L.H. Zhang, Optic Express 19 (S2) (2011) A201.
[10] H.R. Hoekstra, K.A. Gingerich, Science 14 (1964) 1163.
[11] H.R. Khosroshahi, K. Edalati, H. Emami, E. Akiba, Z. Horita, M. Fuji, Inorg. Chem. 56 (2017) 2578.
[12] A. Camenzind, R. Strobel, S.E. Pratsinis, Chem. Phys. Lett. 415 (2005) 193.
[13] M.G. Ivanov, I.V. Krutikova, U. Kynast, M. Lezhnina, I.S. Puzyrev, Opt. Mater. 74 (2017) 67.
[14] A.I. Kostyukov, Vl N. Snytnikov, A.V. Zhuzhgov, S.V. Cherepanova, A. V. Ishchenko, M.G. Baronskiy, V.N. Snytnikov, J. Alloys Compd. 815 (2020), 152476.
[15] A. Kostyukov, M. Baronskiy, A. Rastorguev, V. Snytnikov, Vl Snytnikov, A. Zhuzhgov, A. Ishchenko, RSC Adv. 6 (3) (2016) 2072.
[16] T. Schleid, G. Meyer, J. Less Common Met. 149 (1989) 73.
[17] Bruker AXS Topas V4, General Profile and Structure Analysis Software for Powder Diffraction Data. – User's Manual, Bruker AXS, Karlsruhe, Germany, 2008.
[18] V.V. Atuchin, A.S. Aleksandrovsky, O.D. Chimitova, T.A. Gavrilova, A.S. Krylov, M. S. Molokeev, A.S. Oreshonkov, B.G. Bazarov, J.G. Bazarova, J. Phys. Chem. C 118 (2014), 15404.
[19] Y. Kumar, M. Pal, M. Herrera, X. Mathew, Opt. Mater. 60 (2016) 159.